The Astrophysical Journal, 728:22 (7pp), 2011 February 10 doi:10.1088/0004-637X/728/1/22

RHESSI IMAGING SURVEY OF γ-RAY BREMSSTRAHLUNG EMISSION IN SOLAR FLARES

S. Ishikawa[1,2], Säm Krucker[3,4], T. Takahashi[1,2], and R. P. Lin[3,5,6]
[1] Institute of Space and Astronautical Science, Japan Aerospace Exploration Agency, Sagamihara, Kanagawa 252-5210, Japan; ishikawa@astro.isas.jaxa.jp
[2] Graduate School of Science, University of Tokyo, Bunkyo, Tokyo 113-0033, Japan
[3] Space Science Laboratory, University of California, Berkeley, CA 94720, USA
[4] Institute of 4D Technologies, University of Applied Sciences Northwestern Switzerland, 5210 Windisch, Switzerland
[5] Department of Physics, University of California, Berkeley, CA 94720-7300, USA
[6] School of Space Research, Kyung Hee University, Yongin, Gyeonggi 446-701, Republic of Korea
Received 2010 October 19; accepted 2010 November 29; published 2011 January 14

ABSTRACT

We present a high-energy (>150 keV) imaging survey of all solar γ-ray flares observed by the *Reuven Ramaty High Energy Solar Spectroscopic Imager* (*RHESSI*) to study bremsstrahlung emission from relativistic electrons. Using *RHESSI* rear segment data, images in the energy range from 150 to 450 keV integrated over the total duration of the impulsive phase of the flare are derived. Out of the 29 γ-ray peaks in 26 *RHESSI* flares, we successfully obtained images for 21 γ-ray peaks in 20 flares. The remaining eight peaks have >150 keV fluences of less than a few hundred photons per cm^2 and counting statistics are too poor for detailed imaging. The flux ratio of the footpoint sources is found to be similar at 50 keV and above 150 keV, indicating that relativistic electrons are present in both footpoints of the flare loop. No correlation between the footpoint separation and the fluence ratio of the 2.2 MeV line and the >300 keV photons is found. This indicates that the relative efficiency of proton to electron acceleration does not depend on loop length, as could have been expected from stochastic acceleration models. As previously reported, the three flares with the best counting statistics show not only footpoint emission, but also a coronal γ-ray bremsstrahlung source. For events with lower counting statistics, no coronal source could be identified. However, instrumental limitation could easily hide a coronal source for events with lower statistics, suggesting that coronal γ-ray bremsstrahlung sources are nevertheless a general feature of γ-ray flares.

Key words: Sun: flares – Sun: particle emission – Sun: X-rays, gamma rays

Online-only material: color figures

1. INTRODUCTION

In solar flares, it is well known that electrons are accelerated to relativistic energy up to tens of MeV and ions up to tens of GeV. Magnetic reconnection processes are thought to play an essential role in the release of magnetic energy and the particle acceleration process. Particles accelerated near reconnection points in the corona travel along magnetic field lines until they reach the chromosphere, where they are thermalized by collisions. Bremsstrahlung emissions of energetic electrons produce hard X-ray (HXR) emissions mainly in footpoints of flare loops. Bremsstrahlung emissions from the corona are generally fainter (for review see Krucker et al. 2008b), but coronal emissions are nevertheless present in all flares (e.g., Krucker & Lin 2008; Tomczak 2009). In particular, above-the-loop-top HXR sources support the idea of a coronal acceleration site related to magnetic reconnection (e.g., Masuda et al. 1994; Krucker et al. 2010). HXR observations are therefore crucial tools for studying electron acceleration in solar flares.

The *Reuven Ramaty High Energy Solar Spectroscopic Imager* (*RHESSI*) is the first solar mission for HXR and gamma-ray imaging spectroscopy up to 17 MeV (Lin et al. 2002). *RHESSI* has observed 26 γ-ray flares (i.e., flares with emission above 300 keV) so far (Shih et al. 2009a). Non-thermal bremsstrahlung emissions in the γ-ray range are produced by relativistic electrons. Several single event studies of *RHESSI* imaging above 150 keV have been published. In the flare of 2002 July 23, the location of electron bremsstrahlung emissions in 300–500 keV band and the neutron capture line of 2.223 MeV are spatially separated by $20'' \pm 6''$, implying a difference in acceleration site and/or transport effects for electrons and ions (Hurford et al. 2003). In Hurford et al. (2006), 200–300 keV images from electrons and 2.223 MeV line images from ions in the 2003 October 28 and 29, November 2 flares are compared. The October 28 event, which has the best counting statistics by far, shows two footpoints at 2.223 MeV that originate from the flare ribbon seen in extreme ultraviolet. The electron footpoints are again displaced by $17'' \pm 5''$, but electron and ion accelerations appear to happen on flare loops of similar length. In the 2005 January 20 flare, two footpoints are clearly seen at 250–500 keV, with a coronal source appearing during the decay phase (Krucker et al. 2008a). The limb event of 2005 September 7 shows a similar source, unambiguously locating these sources in the corona. These coronal γ-ray sources show that relativistic electrons stay long enough in the corona to lose their energy by collision in the corona, while lower energy electrons precipitate much faster.

In this paper, an imaging survey of all *RHESSI* γ-ray flares is presented and discussed.

2. OBSERVATIONS

RHESSI is a satellite mission to observe solar flares through imaging and spectroscopy in the HXR and γ-ray bands from 3 keV to 17 MeV (Lin et al. 2002). The *RHESSI* instrument is a rotating modulation collimator obtaining images by Fourier reconstruction of time modulation produced as the satellite rotates (Hurford et al. 2002). *RHESSI* has nine germanium detectors and corresponding nine bi-grid subcollimators (Smith et al. 2002). Electrically, each detector has two segments (front and rear) and signals from each segment are read out separately. Front segments have a thickness of ~1 cm and have sensitivity

Table 1
Table of Properties and Imaging Results of Analyzed Flare Events

Date and Interval (UT)	*GOES* Class	Location ($''$)	>150 keV Fluence (photons cm^{-2})	Number of FPs (50–100 keV)	(150–450 keV)	Footpoint Separation ($''$)	Pile-up (%) (50–100 keV)
2002 Feb 26 10:26:00-10:28:01	C9.6	(930, −230)	179 ± 35	1	...		3
2002 May 31 00:06:00-00:09:02[a]	M2.4	(−820, −480)	364 ± 34	2	...	33[e]	1
2002 Jul 20 21:07:00-21:12:03[a]	X3.3	(−940, −200)	2593 ± 67	...	...		19
2002 Jul 23 00:27:00-00:30:02	X4.8	(−870, −230)	25285 ± 81	2	2	27	18
2002 Aug 20 08:24:00-08:28:02	M3.4	(580, −260)	452 ± 70	3	...		7
2003 Apr 26 08:05:00-08:08:22	M7.0	(850, 330)	582 ± 36	1	1		3
2003 May 27 23:04:00-23:08:02	X1.4	(270, −100)	52.2 ± 2.9	1	1		4
2003 Jun 17 22:53:00-22:56:02	M6.8	(−790, −140)	3281 ± 45	2	2	35	6
2003 Oct 28 11:08:00-11:11:02[b, c]	X17	(−90, −370)	>98514 ± 127	2	2	94	58
2003 Oct 29 20:39:00-20:47:05[d]	X10	(90, −380)	...	2	2	44	39
2003 Nov 2 17:16:00-17:24:05[c]	X8.3	(770, −340)	74592 ± 172	2	2	37	43
2003 Nov 3 09:48:00-09:52:02	X3.9	(920, 130)	2419± 55	2	1	17[e]	35
09:58:00-10:01:42[c]			855 ± 51	2	2	40	21
2004 Jan 6 06:22:00-06:24:01[a]	M5.8	(−970, 90)	654 ± 16	2	2	75	3
2004 Jul 15 01:37:00-01:40:02	X1.8	(−750, −190)	28.7 ± 3.1	1	...		6
2004 Jul 15 18:21:00-18:24:02	X1.6	(−650, −230)	96.7 ± 5.3	1	1		13
2004 Jul 16 02:02:00-02:05:02	X1.3	(−610, −230)	17.5 ± 4.0	2	...	25[e]	8
2004 Nov 10 02:08:00-02:12:02	X2.5	(700, 90)	3756 ± 72	2	2	16	6
2005 Jan 15 22:44:00-22:47:02[c]	X2.6	(110, 310)	>16597 ± 163	2	1	39[e]	7
2005 Jan 17 09:43:00-09:46:02	X3.8	(440, 300)	16512 ± 120	2	2	40	9
2005 Jan 19 08:12:00-08:17:03	X1.5	(700, 280)	3996 ± 72	2	1	43[e]	8
08:24:00-08:30:04			11723 ± 98	2	1	68[e]	2
2005 Jan 20 06:44:00-06:52:05	X7.1	(820, 250)	204495 ± 312	2	2	35	32
2005 Aug 25 04:36:00-04:40:02	M6.4	(−920, 120)	3525 ± 52	1	2	17	5
2005 Sep 7 17:43:00-17:47:02[a, b, c, d]	X17	(−960, −210)	...	0	1		42
2005 Sep 9 20:04:00-20:12:05[b]	X6.2	(−830, −270)	>945 ± 12	2	1	87[e]	9
2005 Sep 10 21:33:00-21:36:02	X2.1	(−660, −260)	200 ± 5.8	2	1	24[e]	5
21:55:00-21:58:02[c]			>249 ± 4.4	...	...		5
2005 Sep 13 23:18:00-23:22:02	X1.7	(−30, −300)	51.4 ± 4.8	2	...	21[e]	22

Notes.
[a] Occurred near or over the solar limb (Shih et al. 2009a).
[b] Missing beginning data (Shih et al. 2009a).
[c] Missing end data (Shih et al. 2009a).
[d] Poor background subtraction (Shih et al. 2009a).
[e] Determined by the 50–100 keV image (others are by the 150–450 keV image).

to low-energy (<200 keV) photons, while rear segments with a thickness of ∼7 cm are used for high-energy (>200 keV) photons. The effective area of the front and rear segments is comparable for ∼200 keV. Therefore, rear segments of the detectors are needed to observe high energy emissions from relativistic electrons. Since the front segments act as a shield for the rear segments, the rear segment data are almost pile-up free. On the other hand, due to the large volumes of the rear segments, the rear background is higher by one order of magnitude than the front background (Smith et al. 2002). Each pair of grids has a different slit pitch and thickness. The different grid pitches give spatial resolutions from $2''$ to $183''$, while the thickness of the grids determine the energy up to which imaging works. In the γ-ray range (>300 keV), grids 1 and 2 are not thick enough to modulate counts. While grid 3 works up to ∼400 keV, all others work up to at least ∼600 keV (Hurford et al. 2002). For our survey, we use rear segment data of subcollimators 3–9 or subcollimators 4–9 depending on image quality. For comparison, we also make images with the same subcollimator using front segment data at lower energy (50–100 keV). We use the CLEAN algorithm (Hurford et al. 2002), providing an FWHM resolution of ∼$10''$ for subcollimators 3–9 and ∼$17''$ for subcollimators 4–9.

2.1. Event Selection

We analyzed 26 γ-ray flares observed by *RHESSI* from the event list of Shih et al. (2009a). This list contains all events seen above 300 keV. Hence, we exclude rear segment flare events seen only below 300 keV. However, these events are expected to be small. Since some of the events seen above 300 keV already do not have good statistics to provide detailed imaging (see Section 2.2), omitting rear segment flare events seen below 300 keV does not influence the results presented here. To enhance statistics, we make flare-integrated images over all rear segment counts (>150 keV). Table 1 shows the list of analyzed events and their properties. The *GOES* class of these events varies from C9.6 to X17. The time intervals shown are determined from light curves of >150 keV of the rear segments. For imaging, we exclude times of attenuator changes. As described in Shih et al. (2009a), two clearly separated peaks are seen in three flares. For these events, we analyzed the two time intervals separately.

2.2. Imaging Results

As image quality depends heavily on counting statistics, we first discuss the >150 keV fluence of the selected events.

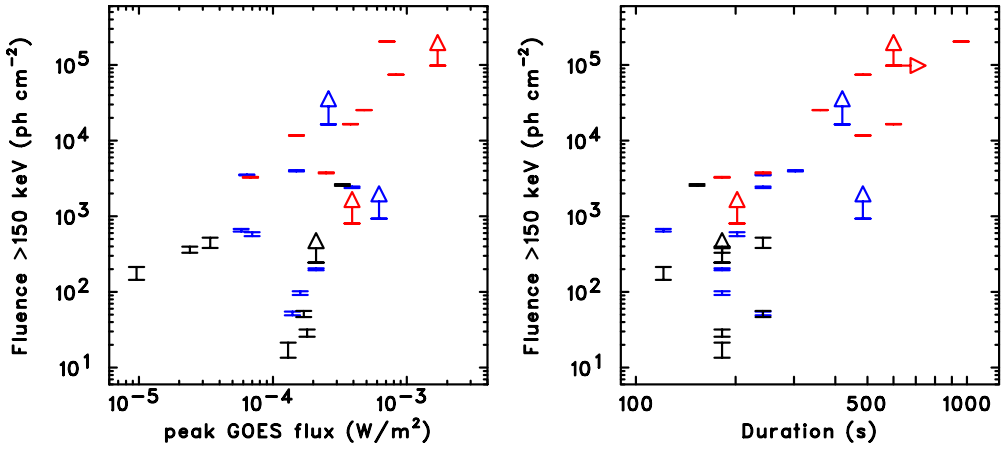

Figure 1. Left: fluence >150 keV vs. *GOES* flux. Right: fluence >150 keV vs. duration. Colored points indicated that a detailed image could be obtained in the 150–450 keV band (events with a double source structure are shown in red, while events with a single source are shown in blue). For the remaining events (black) no detailed imaging information could be derived. Events for which only lower limits of the total fluence are available are marked by arrows (see Shih et al. 2009a for details).

(A color version of this figure is available in the online journal.)

Figure 1 shows the >150 keV fluence against the *GOES* peak soft X-ray flux and total duration of the >150 keV emission for all of the selected events. Events for which a detailed image could be reconstructed are shown in color (21 out of 29 time intervals). These events have a >150 keV fluence of at least several hundred photons per cm^2. For the remaining events, counting statistics are too poor for detailed imaging, and only a centroid location of the >150 keV flux could be determined. The events given in red reveal two footpoints, while events shown in blue show a single source (Figure 2). Again, there is a dependence on counting statistics. Two-footpoint events have higher fluences than single source events, suggesting that events with a single source could have a second footpoint that is hidden in the noise. Imaging at lower energies with much better statistics confirms this, showing several events with two footpoints (e.g., 2005 January 19). Some events with a single source at >150 keV, however, are spatially unresolved (e.g., 2003 April 26). Taking the different dynamic ranges of the 50 keV and 150–450 keV images into account, the source morphology at both energy ranges is generally the same. Slight differences in position of two footpoints, such as seen in the 2004 January 1 event where the weaker footpoint at higher energies is shifted relative to the location of the footpoint at 50–100 keV, are an artifact of the limited counting statistics. The main difference between the front and rear images can be attributed to pile-up. In large flares such as those investigated here, the large number of thermal photons detected produce significant pile-up events. As most low energy photons are absorbed in the front segments, almost all pile-up counts are registered in the front segment. Rear segment data generally do not suffer from pile-up effect (Smith et al. 2002). For our set of events, the fraction of pile-up counts are estimated to be between a few percent up to 60% (see Table 1 and top left corner of images shown in Figure 2). These values are rough estimates averaged over a spin period (~4 s). Hence, during peak times in the modulation pattern, the fraction of pile-up counts is significantly higher than the reported average value. Although the effects of pile-up on imaging are complex, to first order, pile-up events by two thermal photons produce an image at the location of the thermal source at double the energy. Since the 50–100 keV energy range is generally dominated by non-thermal footpoint emissions from the chromosphere without any thermal contribution, pile-up effect can produce a spurious coronal source. This is most clearly seen in the 2003 October 28 event with the enormous pile-up fraction of 58% (we note that our simple pile-up estimate is likely failing for this extremely high count rate) where the 50–100 keV emission shows an extended coronal source, while the rear image shows mostly footpoint emission. A spurious coronal source is also visible in the 2003 November 2 and November 3 event. In the 2005 September 7 event with 43% pile-up, a coronal HXR source is imaged with both front and rear segment data, suggesting that only part of the coronal emission at 50–100 keV is produced by pile-up.

2.3. Ratio of Footpoint Intensities

To investigate spectral differences of the two footpoints, we calculated fluxes of each footpoint in two energy bands (50–100 keV and 150–450 keV). Previous studies of spectral differences in HXR spectral indices below 100 keV showed that spectral differences are frequently observed. However, the differences are generally small, with the spectral index differing by less than 0.6 (Emslie et al. 2003; Saint-Hilaire et al. 2008). While Emslie et al. (2003) suggested that the difference in column density in the two legs of the flare loop could produce the difference in spectral slope, Saint-Hilaire et al. (2008) noted that significant coronal HXR emission would be produced in such a case, excluding different column densities as an explanation for most events. Other explanations of the asymmetry in the footpoint spectra involve asymmetrical acceleration, non-uniform target ionization, and magnetic mirroring (see Saint-Hilaire et al. 2008 for discussion).

In the following, we check if the asymmetry also holds for spectra above 100 keV. We define the footpoint with higher flux in 50–100 keV as "footpoint 1," and the weaker footpoint as "footpoint 2," and compute the flux ratio of "footpoint 2" to "footpoint 1." Flux ratios of 50–100 and 150–450 keV are plotted in the left panel of Figure 3. The absence of ratios smaller than 0.2 reflects the limited dynamic range. Nevertheless, the footpoint ratios below and above 100 keV are roughly proportional. In the right panel of Figure 3, the power-law indices of each footpoint are plotted. Most of the events show similar spectra for both footpoints, with a tendency

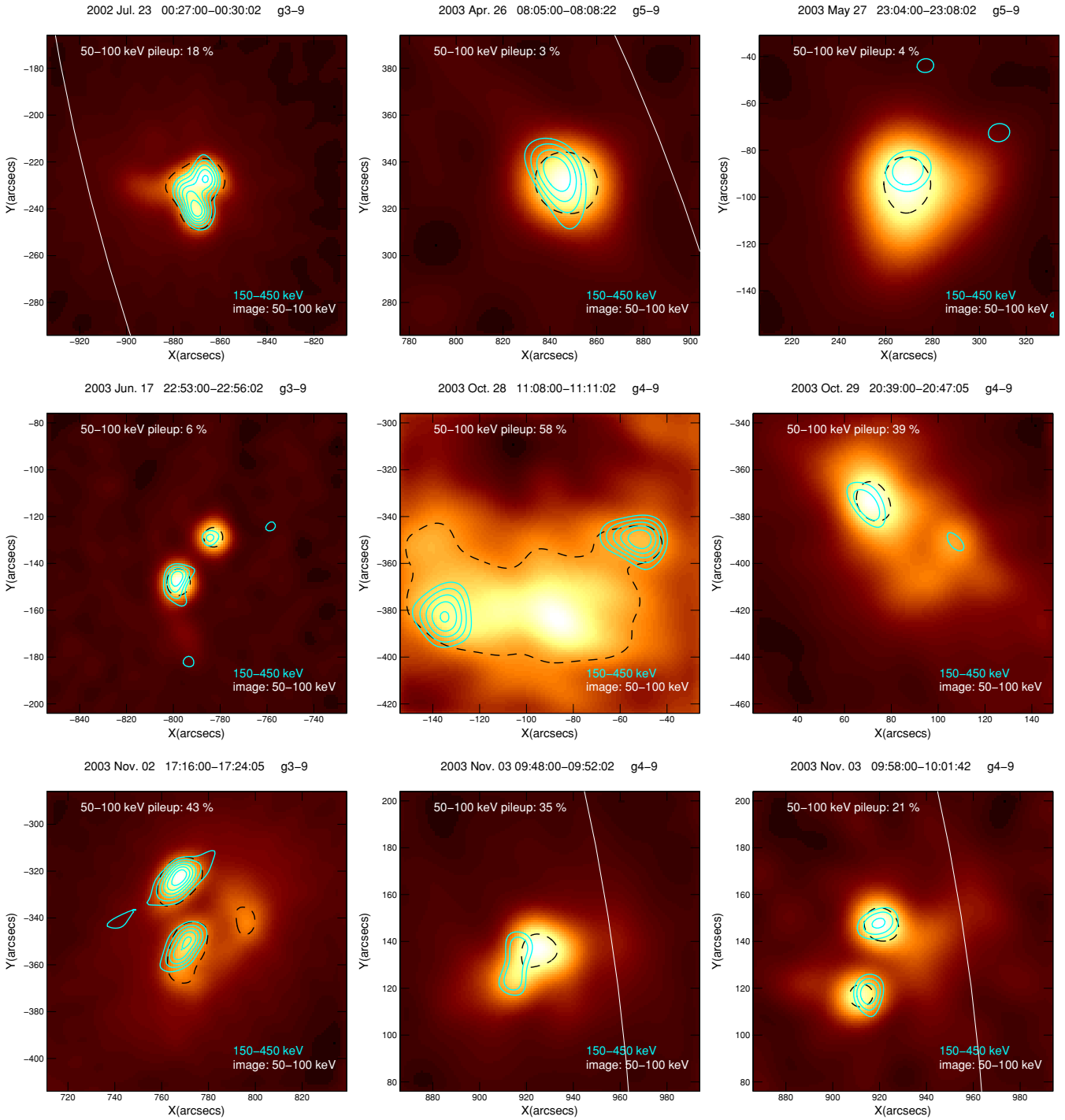

Figure 2. 150–450 keV contours (cyan) over 50–100 keV images of events that successfully imaged in 150–450 keV. The contour levels of 90% and 80% are shown, and 70%, 60%, 50%, and/or 40% are shown if the statistics are sufficient. For comparison, the black dashed contour shows the 50–100 keV image at the lowest percentage level used for the 150–450 keV contour plot. The subcollimators used are given in the title of each plot (the same subcollimators are used for both energy ranges).

(A color version of this figure is available in the online journal.)

that the stronger footpoint has a slightly softer spectrum (8 out of the 10 events). However, the difference derived from the eight events with a softer spectrum is only 1.9 σ. Previous studies do not report such a correlation (Sakao et al. 1996; Saint-Hilaire et al. 2008). Besides that, the results regarding the footpoint asymmetry are similar to what has been found at lower energies (Emslie et al. 2003; Saint-Hilaire et al. 2008), and it indicates that relativistic electrons penetrate at both footpoints at similar rates.

For the seven events that occurred near disk center (see Table 1), we estimated the magnetic field strength at the two footpoints using *SOHO*/MDI magnetograms (Scherrer et al. 1995). In four out of the seven events, the footpoints with higher fluxes in the 50–450 keV band have higher magnetic field strength. The brighter footpoints have lower magnetic fields in the remaining three events. Hence, there is no significant correlation within this limited number of events. To further investigate the relation between HXR intensity and magnetic

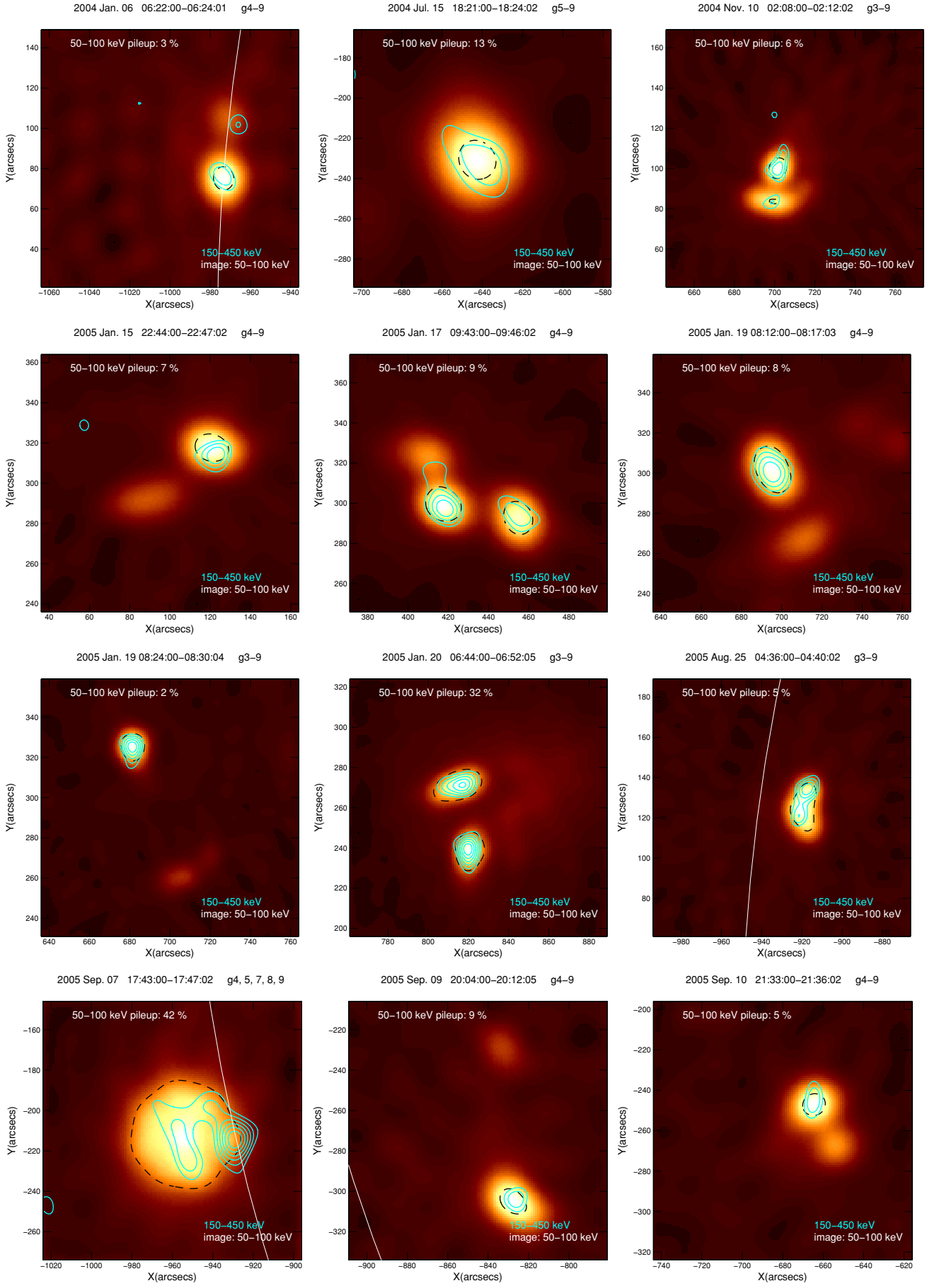

Figure 2. (Continued)

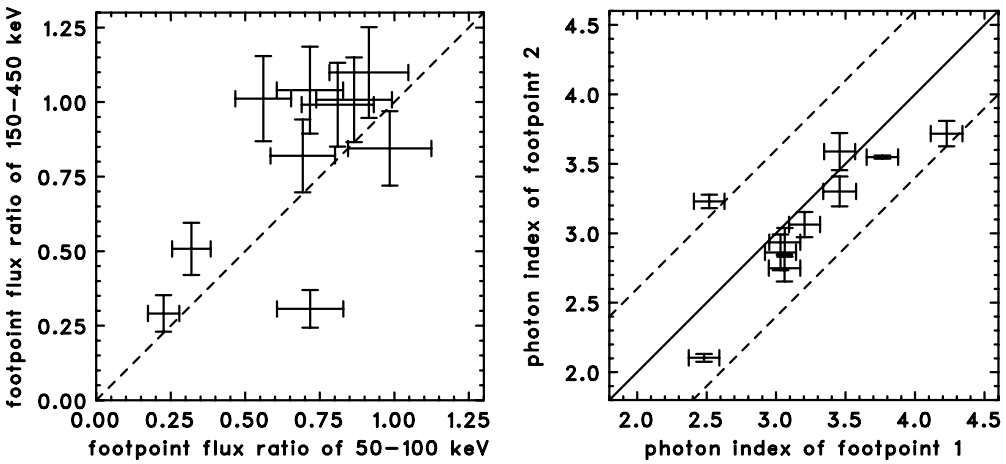

Figure 3. Left: correlation of the footpoint flux ratios at 50–100 keV and 150–450 keV. Right: correlation of the photon spectral index of each footpoint. The dashed line corresponds to a spectral difference of 0.6.

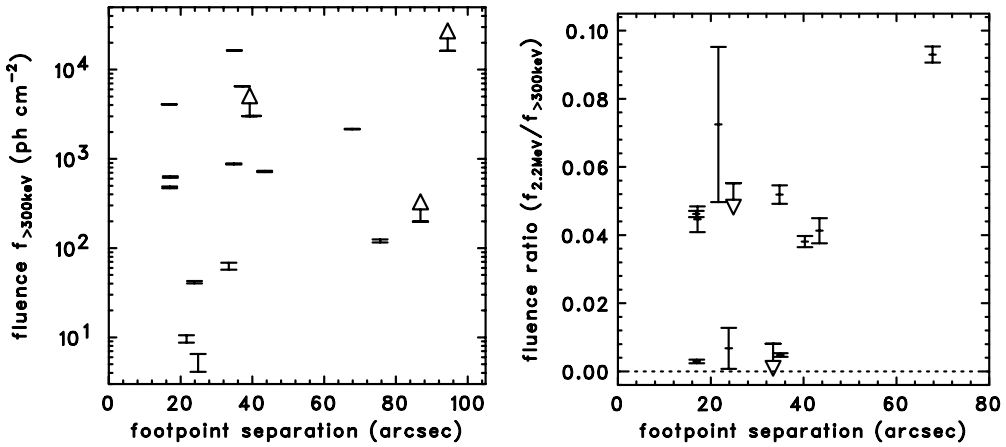

Figure 4. Left: fluence >300 keV vs. footpoint separation. Right: fluence ratio of 2.2 MeV and >300 keV vs. footpoint separation. Fluences are from Shih et al. (2009a) and arrows again mark lower and upper limits.

field strength, a larger sample of events should be considered including the much more numerous events seen at lower energies.

2.4. Separation of Footpoints

Stochastic acceleration models of impulsive flares predict that the fractions of accelerated protons and electrons are determined by the size scale of the acceleration region (Miller 2000). In Emslie et al. (2004), a relation between the scale length of acceleration and acceleration rates of electrons and protons is derived. Assuming a constant acceleration volume of 10^{27} cm^3, the proton acceleration rate increases for spatial scale increasing from 10^8 to 10^9 cm, while the electron acceleration rate decreases. *RHESSI* observations of the 2003 October 28 flare show that electron and proton acceleration occur on flare loops of similar size that are spatially displaced by $(\sim 12 \pm 4) \times 10^8$ cm (Hurford et al. 2006). Here, we investigate if the relative acceleration efficiency of electrons and protons depends on the length of the flare. We use the ratio of the 2.2 MeV fluence to the >300 keV fluence as a measure of the proton-to-electron acceleration efficiency. Furthermore, we assume that the flare loop length scales in the same way as the length of the acceleration region (see Emslie et al. 2004 for a detailed description) and we approximate the flare loop length by the footpoint separation. To avoid problems with spurious sources produced by pile-up, we use the rear segments for the largest events to determine the footpoint separation. For smaller events where pile-up effects are negligible, we calculate footpoint separations by using data from front segments. Figure 4 shows the footpoint separation against the >300 keV fluences (left) and the fluence ratio of 2.2 MeV to >300 keV. The values of the fluences are taken from Shih et al. (2009a). No obvious correlation is found in Figure 4. The only notable fact is that the event with the largest footpoint separation (2003 October 28) is the event with the highest ratio.

2.5. Coronal γ-ray Sources

Coronal γ-ray bremsstrahlung sources are reported for the three *RHESSI* γ-ray flares with the best counting statistics (Krucker et al. 2008a). These sources are most visible in the impulsive phase of the flare during the decay of the non-thermal HXR emission. The observed coronal emission decays more slowly and has a harder spectrum than the footpoint emission, making it easier to detect these sources after the HXR peak time. We checked the entire sample of our events for coronal emissions, in particular during the decay phase of the HXR peak. However, no further event with a coronal γ-ray bremsstrahlung source has been found. For most of the events this can be attributed to low counting statistics. The only candidates with relatively good counting statistics, but without a detectable

coronal source >150 keV, are the events of 2002 July 23 and 2003 November 2. However, these two events also have about three times fewer >150 keV counts than the 2005 January 20 flare discussed in Krucker et al. (2008a). Furthermore, these two events are rather compact compared to the 2005 January 20 flare, where the footpoints and the coronal γ-ray source are separated by $\sim 40''$, making it difficult to image a coronal contribution. Hence, the absence of any further examples of coronal γ-ray bremsstrahlung sources is probably due to observational limitations.

3. SUMMARY AND CONCLUSIONS

Using *RHESSI* rear segment data, we analyzed flare-integrated images of all *RHESSI* γ-ray flares with high enough counting statistics in the energy band from 150 to 450 keV. We report the following findings.

1. The intensity ratios of footpoints at 50–100 keV and 150–450 keV are found to be similar. This indicates that relativistic electrons penetrate at both ends of the flare loop at similar rates. Hence, transport effects from a coronal acceleration site appear to be similar for semi-relativistic electrons producing the 50 keV emission as for relativistic electrons producing the >150 keV emission.
2. There is no obvious correlation between the footpoint separation and the ratio of 2.2 MeV to >300 keV fluence. Hence, the relative acceleration efficiency of electrons and protons does not depend on flare loop length. Such a correlation is proposed to be an indicator for stochastic acceleration models. However, not finding a correlation could also simply be because the spatial scale of the acceleration site does not scale with the loop length.
3. Coronal γ-ray sources are only seen for the three events with best counting statistics (Krucker et al. 2008a). However, the absence of coronal sources for the other events could be due to observational limitations.

While the *RHESSI* imaging concept has been proven to successfully work in the γ-ray range, the limited counts available for most of the detected events make it possible to obtain flare-integrated images only for the few largest events (Hurford et al. 2003, Hurford et al. 2006; Krucker et al. 2008a). To make a breakthrough from the observational side, the sensitivity of a future instrument needs to be improved significantly, preferably by two orders of magnitude. The GRIPS balloon project (Shih et al. 2009b) is a first step toward a future high-sensitivity imaging spectrometer in the γ-ray range.

We thank Lindsay Glesener and Pascal Saint-Hilaire for their comments. The work was supported through NASA contract NAS 5-98033 for *RHESSI*, a Grant-in-Aid for JSPS Fellows from Japan Society for the Promotion of Science, and the Global Center of Excellence Program "the Physical Sciences Frontier," Ministry of Education, Culture, Sports, Science and Technology, Japan. R. Lin was also supported in part by the WCU Grant (R31-10016) funded by the Korean Ministry of Education, Science, and Technology.

REFERENCES

Emslie, A. G., Kontar, E. G., Krucker, S., & Lin, R. P. 2003, ApJ, 595, L107
Emslie, A. G., Miller, J. A., & Brown, J. C. 2004, ApJ, 602, L69
Hurford, G. J., Schwartz, R. A., Krucker, S., Lin, R. P., Smith, D. M., & Vilmer, N. 2003, ApJ, 595, L77
Hurford, G. J., Krucker, S., Lin, R. P., Schwartz, R. A., Share, G. H., & Smith, D. M. 2006, ApJ, 644, L93
Hurford, G. J., et al. 2002, Sol. Phys., 210, 61
Krucker, S., Hudson, H. S., Glesener, L., White, S. M., Masuda, S., Wuelser, J.-P., & Lin, R. P. 2010, ApJ, 714, 1108
Krucker, S., Hurford, G. J., MacKinnon, A. L., Shih, A. Y., & Lin, R. P. 2008a, ApJ, 678, L63
Krucker, S., & Lin, R. P. 2008, ApJ, 673, 1181
Krucker, S., et al. 2008b, A&ARv, 16, 155
Lin, R. P., et al. 2002, Sol. Phys., 210, 3
Masuda, S., Kosugi, T., Hara, H., Tsuneta, S., & Ogawara, Y. 1994, Nature, 371, 495
Miller, J. A. 2000, in ASP Conf. Ser. 206, High Energy Solar Physics Workshop—Anticipating HESSI, ed. R. Ramaty & N. Mandzhavidze (San Francisco, CA: ASP), 145
Saint-Hilaire, P., Krucker, S., & Lin, R. P. 2008, Sol. Phys., 250, 53
Sakao, T., Kosugi, T., Masuda, S., Yaji, K., Inda-Koide, M., & Makishima, K. 1996, Adv. Space Res., 17, 67
Scherrer, P. H., et al. 1995, Sol. Phys., 162, 129
Shih, A. Y., Lin, R. P., & Smith, D. M. 2009a, ApJ, 698, L152
Shih, A. Y., et al. 2009b, AAS/Solar Physics Division Meeting, 40, 18.10
Smith, D. M., et al. 2002, Sol. Phys., 210, 33
Tomczak, M. 2009, A&A, 502, 665